Elastic and magnetic properties of epitaxial MnAs layers on GaAs

F. Iikawa,[1,2,*] P. V. Santos,[1] M. Kästner,[1] F. Schippan,[1] and L. Däweritz[1]
[1]*Paul-Drude-Institut für Festkörperelektronik, Hausvogteiplatz 5–7, 10117 Berlin, Germany*
[2]*Instituto de Física "Gleb Wataghin," UNICAMP, Campinas-SP, CP-6165, 13083-970, Brazil*
(Received 31 July 2001; revised manuscript received 11 March 2002; published 22 May 2002)

We have investigated the elasto- and magneto-optical properties of MnAs layers epitaxially grown on (001) GaAs for temperatures around the structural (hexagonal/orthorhombic) and magnetic (ferromagnetic/paramagnetic) phase transition of MnAs at $T_c \sim 40\,^{\circ}\mathrm{C}$. The phase transition is accompanied by a large variation of the MnAs lattice parameter a of $\sim 1\%$, which induces a strong and anisotropic strain field in the MnAs/GaAs heterostructures. The latter was measured by detecting the optical anisotropy induced on the GaAs substrate by means of polarization-sensitive light transmission measurements. The experimental results show clear evidence for the quasi-uniaxial strain induced on the GaAs substrate during the phase transition, which extends over a temperature range of $\sim 30\,^{\circ}\mathrm{C}$ in the MnAs/GaAs heterostructures. The strain levels are well reproduced by an elastic model for the heterostructures which assumes that the strain is transferred across the MnAs/GaAs interface without relaxation. The elastic properties during the phase transition were compared to the average magnetization probed using a SQUID magnetometer and to the magnetization near the front and the back surfaces of the MnAs films detected using the magneto-optical Kerr effect. The smaller temperature range of the phase transition observed in the magneto-optical Kerr effect measurements indicates a lower stability of the ferromagnetic phase near the surface of the MnAs layers.

DOI: 10.1103/PhysRevB.65.205328 PACS number(s): 78.20.Ci, 75.60.Nt, 75.70.Ak, 78.20.Hp

I. INTRODUCTION

Epitaxial heterostructures of dissimilar materials with respect to the lattice structure and lattice parameter have been attracting great attention due to their fundamental physical properties as well to the possibility of combining different materials in monolithic integrated systems.[1] Typical examples are semiconductor/semiconductor structures, such as wurzite GaN on zinc blende GaAs (Ref. 2) and metal/semiconductor structures, such as hexagonal MnAs on zinc blende GaAs.[3–6] The latter system is particularly interesting, since it allows for the combination of the semiconductor properties of GaAs with the magnetic properties of the MnAs layers, which is a ferromagnetic material with a Curie temperature T_c of $\approx 40\,^{\circ}\mathrm{C}$.[7–12]

Recently, different groups have reported[3–6] the epitaxial growth of MnAs on GaAs using low temperature ($\sim 200\,^{\circ}\mathrm{C}$) molecular beam epitaxy (MBE). The epitaxial growth requires an appropriate arrangement of the interface bonds in order to accommodate the large mismatch in lattice constants between the two crystalline structures. It has been found that for structures grown on (001) GaAs, the lattice mismatch can be minimized if the c-axis of the MnAs layers is oriented along one of the $\langle 110 \rangle$ directions of the substrate surface.[1,5,13,14] In the so-called A-orientation, the [11.0] axis (a-axis) of the MnAs layer is parallel to the $x=[110]$ axis of GaAs, while the $c=[00.1]$ MnAs axis is parallel to the $y=[1\bar{1}0]$ GaAs direction. In this configuration, the easy magnetization of the MnAs layers lies along the a-axis.[6,15]

A second source of lattice strain in MnAs/GaAs structures is associated with the first order magnetic phase transition from the paramagnetic phase with MnP-like orthorhombic structure (β-MnAs) to the NiAs-like hexagonal ferromagnetic phase (α-MnAs) at $T_c \sim 40\,^{\circ}\mathrm{C}$. In bulk MnAs, this phase transition is accompanied by a discontinuous expansion of the lattice in the direction corresponding to the a-axis of the hexagonal phase by $\sim 1\%$.[7,12,16] The lattice expansion is highly anisotropic, no discontinuity is observed in the lattice constant along the hexagonal c-axis.[7,12,16] The phase transition and the lattice expansion can be also induced by an external magnetic field or by external pressure.[8–12] In MnAs/GaAs heterostructures, the MnAs layer is not free to expand, so that extra elastic energy accumulates in the epitaxial structure, which may lead to modifications of its physical properties. In fact, strain effects have been invoked to explain the nonabrupt nature of the ferromagnetic phase transition in MnAs/GaAs heterostructures.[17] In contrast to the first order transition observed in bulk MnAs, the α-MnAs and β-MnAs phases in the heterostructures coexist over a temperature range of more than $20\,^{\circ}\mathrm{C}$.[17] It has been suggested that the strain stabilization of the β-MnAs phase explains the anomalous temperature dependence of the magnetic properties in the heterostructures.[18]

An interesting question is how the strain field induced by the lattice mismatch between MnAs and GaAs distributes across the heterostructure and how it depends on (and effects) the magnetic properties of the MnAs layers. This question is also of large technological interest, since the modification of the magnetic properties of the layers may influence physical effects such as spin transport and spin injection across the MnAs/GaAs interface. In this work, we address this problem by investigating the elastic properties of epitaxial MnAs/GaAs heterostructures during the ferromagnetic phase transition and its effects on the magnetic properties of the MnAs layers. For that purpose, we have first studied the anisotropic strain distribution in the MnAs/GaAs structures induced by the expansion (or contraction) of the MnAs layer during the phase transition. This was accomplished by detecting the anisotropy of the optical properties of the sub-

strate induced by the strain field by means of polarization-sensitive light transmission measurements. The high sensitivity of this technique allows for the detection of relative changes $\Delta n/n < 10^{-6}$, where n is the average refractive index and Δn is the difference between the refractive index for light linearly polarized along two perpendicular directions.[19] In GaAs, the anisotropy in n can be directly related to the strain field using the well-known photoelastic coefficients.[20,21] The polarization technique used here to probe the elastic properties is complementary to those based on the measurement of the radius of curvature of the film/substrate structure.[22,23] The experimental results compare well with an elastic model for the strain distribution in the heterostructure. From these studies, we conclude that the strain field induced during the MnAs phase transition is transferred across the MnAs/GaAs interface without relaxation, thus indicating that there is negligible strain relief due to the creation of misfit dislocations.

In the second part of the studies, we address the effects of an applied magnetic field on the physical properties of the MnAs/GaAs structures. We verify that the strain field does not depend on an applied magnetic field for field amplitudes up to 200 Oe. This result is attributed to the high magnetic anisotropy of the MnAs layers, which constrains the magnetization to be parallel to the MnAs a-axis for low applied fields. Since magnetostriction only depends on the direction (and not on the sign) of the field,[24] it has the same value for domain oriented by the applied field along the $+a$ or $-a$-MnAs axes. Furthermore, the magnetic properties of the MnAs surface measured by magneto-optical Kerr rotation (MOKE) experiments show a narrower temperature range for the phase transition as compared to the bulk magnetization and to the optical transmission measurements, which is attributed to a lower stability of the ferromagnetic phase near the surface of the MnAs layers.

This manuscript is organized as follows: In Sec. II, we present a model for the strain distribution in MnAs/GaAs heterostructure and for the accompanying modification of the optical properties of the substrate. This model constitutes the basis of the optical techniques used to detect the strain, which are described in Sec. III. Section IV summarizes the experimental results on the strain distribution across the MnAs/GaAs heterostructures and of its relationship to the magnetic properties of the MnAs layers. These results are discussed in Sec. V. The main conclusions of this work are summarized in Sec. VI.

II. STRAIN IN MnAs/GaAs HETEROSTRUCTURES

The strain field induced by an epitaxial MnAs film with A-orientation on the substrate has two sources. The first is the mismatch in lattice constants between MnAs and GaAs, which differs along the [110] and $[1\bar{1}0]$ directions in the plane of the interface. The epitaxial alignment of MnAs a-axis with the [110] substrate axis reduces the lattice strain along this direction to less than 10%.[13] The lattice mismatch along the a-axis is further reduced by the formation of misfit dislocations. The large difference between the atomic spacing along the MnAs c-axis and the GaAs $[1\bar{1}0]$ atomic

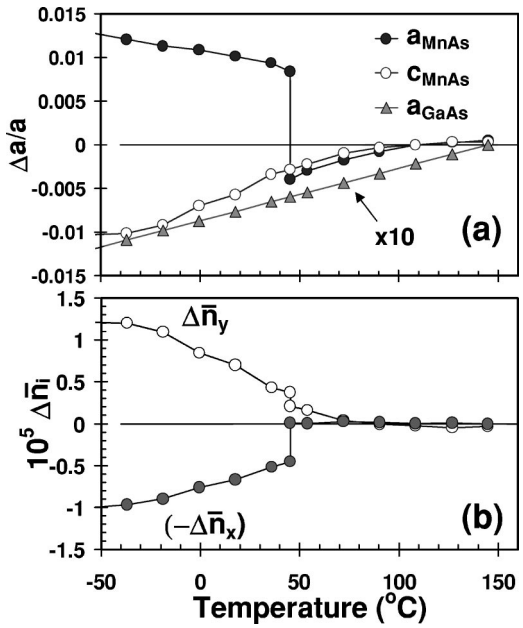

FIG. 1. (a) Temperature dependence of the relative changes $\Delta a/a$ in lattice constant of GaAs (Ref. 20) (a_{GaAs}, scaled by 10) and of the MnAs lattice constants along the a-axis (Ref. 16) (a_{MnAs}) and the c-axis (Ref. 16) (c_{MnAs}). The values are relative to those at $T=150\,^{\circ}\mathrm{C}$, which are given by $a_{\mathrm{MnAs}}(150\,^{\circ}\mathrm{C})=0.368\,273$ nm (Ref. 16), $c_{\mathrm{MnAs}}(150\,^{\circ}\mathrm{C})=0.573$ nm (Ref. 16), and $a_{\mathrm{GaAs}}(150\,^{\circ}\mathrm{C})=0.565\,406$ nm (Ref. 20). (b) Temperature dependence of the anisotropy of the average refractive index $\Delta\bar{n}_y=\bar{n}_z-\bar{n}_x$ and $-\Delta\bar{n}_x=\bar{n}_z-\bar{n}_y$ calculated using the model described in the text for a 0.18 μm-thick MnAs layer on a 245 μm-thick GaAs substrate (corresponding to the thickness sample A in Table I).

planes is partially accommodated by a commensurate atomic arrangement, where every fourth {00.2} MnAs plane coincides with every sixth {220} GaAs plane.[13] The formation of secondary dislocations essentially eliminates the strain arising from lattice mismatch along this direction.

The second source of strain, which will be the subject of the present investigation, is related to the strong temperature dependence of the lattice constants of bulk MnAs. Figure 1(a) displays the temperature dependence of the relative changes in lattice constant $\Delta a/a=[a(T)-a(T=150\,^{\circ}\mathrm{C})]/a(T)$, for $a(T)=a_{\mathrm{MnAs}}$, c_{MnAs}, and a_{GaAs}, in bulk MnAs (Ref. 16) and bulk GaAs (Ref. 20) for temperatures around the MnAs phase transition temperature T_c. We note that, although the qualitative features agree, there are considerable differences in the reported data for the temperature dependence of the lattice constants of bulk MnAs.[7,16,25] For the following discussion, we will concentrate on the data from Ref. 16. The discontinuous increase in lattice spacing along the a-direction of $\sim 1\%$ as the temperature reduces below $T\sim 40\,^{\circ}\mathrm{C}$ is attributed to the transition from orthorhombic to hexagonal phase.[7,8,11,16] The phase transition is also accompanied by an anomalous behavior of the elastic properties.[12,26,27] The thermal expansion coefficients of MnAs are substantially larger than the one for GaAs. The thermal expansion coefficient along the a-axis changes sign for temperatures below the phase transition. Above the phase transition, the coefficients for the a- and c-axis have similar

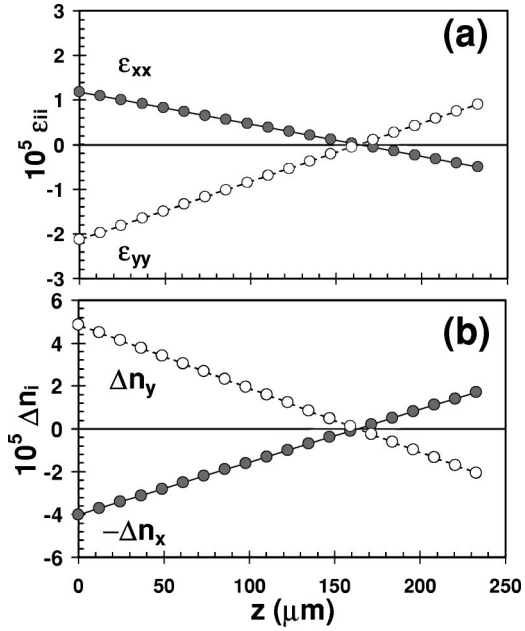

FIG. 2. Depth dependence of (a) the strain components ε_{xx} (dots) and ε_{yy} (circles) and of (b) the refractive index anisotropies $\Delta n_y(=n_z-n_x$, circles) and $-\Delta n_x(=n_z-n_y$, dots) in the GaAs substrate calculated using the strain data of Fig. 1 for a temperature ($T=-40$°C) well below the phase transition.

magnitude. Finally, the second order phase transition from the β-MnAs to the γ-MnAs NiAs-like hexagonal paramagnetic phase, which takes place at ≈ 125 °C,[28] has no appreciable effect on the temperature dependence of the MnAs lattice constants and will, therefore, not be further considered here.

In order to calculate the strain field induced by the temperature changes on the optical properties of the substrate, we will assume that for high temperatures (above 150 °C) the strain field induced by the lattice mismatch is effectively relaxed by dislocations. Below that temperature, it is unlikely that this strain field can be relaxed by mobile dislocations. Therefore, it will be assumed that the strain field below 150 °C is determined by the changes in lattice constant displayed in Fig. 1(a). The strain distribution in the MnAs film and in the GaAs substrate was calculated following the procedure delineated in Refs. 29 and 30. For that purpose, we employed the elastic constants for GaAs reported in Ref. 20 and those for the hexagonal phase of bulk MnAs from Ref. 27. The temperature dependence of the MnAs elastic constants was not taken into account. The results will be displayed relative to a coordinate system with axes $x||[110]$, $y||[1\bar{1}0]$, and $z||[001]$ of GaAs. Due to symmetry, the only nonvanishing strain tensor components are ε_{xx}, ε_{yy}, and ε_{zz}. These components vary linearly with z in the GaAs substrate ($0<z<d_{\mathrm{GaAs}}$) and in the MnAs layer ($-d_{\mathrm{MnAs}}<z<0$), thus leading to a bending of the film–substrate structure.

The dependence of ε_{xx} and of ε_{yy} within the GaAs layer is illustrated in Fig. 2 for a sample consisting of a 0.18 μm thick MnAs layer on a 245 μm-thick GaAs substrate. The calculations were performed for a temperature $T=-40$ °C, which is well below the phase transition temperature. With decreasing temperature, the expansion (compression) of the MnAs lattice along the a- (c-) direction leads to a positive (negative) strain component ε_{xx} (ε_{yy}) at the substrate side of the interface ($z=0$). As a consequence of the bending of the MnAs/GaAs structures, the strain decreases linearly with the distance from the interface and vanishes at the plane $z=166$ μm.

The strain field ε reduces the cubic symmetry of the GaAs substrate. The changes in the dielectric tensor, $\Delta\epsilon$, can be expressed in terms of the elastooptic tensor p according to[21]

$$\Delta\epsilon=-\epsilon_{\mathrm{GaAs}}^2 p:\varepsilon, \tag{1}$$

where ϵ_{GaAs} is the GaAs dielectric constant. For the MnAs/GaAs system, the only nonvanishing components of $\Delta\epsilon$ are $\Delta\epsilon_{xx}$, $\Delta\epsilon_{yy}$, and $\Delta\epsilon_{zz}$. The latter yield directly the anisotropy in the refractive index Δn_i along the main optical axis of the heterostructures, which is defined as

$$\Delta n_i=n_j-n_k, \qquad i,j,k=\text{cyclic permutation of } x,y,z. \tag{2}$$

According to the convention used here, the index i in Δn_i defines the propagation direction of the light beam, while that in n_i specifies the polarization. The n's are defined as $n_x=\sqrt{\epsilon_{\mathrm{GaAs}}+\Delta\epsilon_{xx}}$, $n_y=\sqrt{\epsilon_{\mathrm{GaAs}}+\Delta\epsilon_{yy}}$, and $n_z=\sqrt{\epsilon_{\mathrm{GaAs}}+\Delta\epsilon_{zz}}$. Figure 2(b) displays profiles of Δn_x and Δn_y across the thickness of the substrate calculated using the strain field shown in Fig. 2(a) for a light wavelength $\lambda_L=1000$ nm. The elastooptic coefficients for this wavelength were extracted from Ref. 21.

As will be described in detail in Sec. III B, the strain field induced by the MnAs on the GaAs substrate was determined by measuring the average refractive index anisotropy $\Delta\overline{n_i}$ along the z-direction defined as

$$\Delta\overline{n_i}=\frac{1}{d_{\mathrm{GaAs}}}\int_0^{d_{\mathrm{GaAs}}}\Delta n_i(z)dz. \tag{3}$$

The calculated temperature dependence of $\Delta\overline{n_i}$ ($i=x,y$) for the MnAs/GaAs structure of Fig. 2 is illustrated in Fig. 1(b). Note that the discontinuity in a_{MnAs} at $T_c\sim 40$ °C leads to discontinuities both in $\Delta\overline{n_x}$ and in $\Delta\overline{n_y}$.

III. EXPERIMENTAL DETAILS

A. Sample preparation

MnAs epitaxial layers used in this study were grown on (001) GaAs substrate by molecular beam epitaxy (MBE) at a growth temperature of 250 °C. The growth conditions were optimized to yield MnAs with a preferential A-orientation,[5,13] i.e., with the $a=[11.0]$ MnAs axis (which corresponds to the easy magnetization direction) aligned along the GaAs [110] surface direction. Additional details about the growth and characterization of the samples are reported in Refs. 5 and 13.

The strain field induced by the MnAs layers on the substrate was determined by measuring the optical anisotropy

TABLE I. Properties of the MnAs/GaAs samples investigated in this work. d_{MnAs} and d_{GaAs} denote the thicknesses of the MnAs film and of the GaAs substrate, respectively. $T_{c,\mathrm{min}}$ and $T_{c,\mathrm{max}}$ are the temperature limits of the magnetic phase transition of the MnAs structures measured during sample heating.

Sample	d_{MnAs} (μm)	d_{GaAs} (μm)	$T_{c,\mathrm{min}}$ (°C)	$T_{c,\mathrm{max}}$ (°C)
A	0.18	245	18	48
B	0.10	330	9	43
C	0.25	60	27	53
GaAs	...	350	...	...

generated in the GaAs substrate. For a fixed thickness d_{MnAs} of the MnAs layers, the strain field on the substrate increases with decreasing substrate thickness d_{GaAs}. In order to increase the sensitivity of the measurements, the GaAs substrates were thinned and polished at the back side. After that, pieces with wave guide lengths l_{GaAs} of ≈ 1 mm along the GaAs [110] and the $[1\bar{1}0]$ directions were cleaved to assure good lateral surfaces in- and out-coupling of the light. A 350-μm-thick plain GaAs substrate was used as a reference for the calibration of the experimental setup. The dimensions of the samples used in this work are listed in Table I.

B. Transmission measurements

The strain field induced by the MnAs layers on the substrate was determined by detecting the change in light polarization upon transmission, using the wave guide geometry illustrated in Fig. 3. The complex transmission coefficient t_i for a light beam polarized along direction $i=x,y,z$ is given by

$$t_i = t_{i0} \exp\left[-\imath \frac{2\pi n_i l_{\mathrm{GaAs}}}{\lambda_L} \right], \tag{4}$$

where t_{i0} represents the module of the transmission coefficient, λ_L the light wavelength, and l_{GaAs} is the length of the propagation path through the GaAs substrate. The anisotropy Δn_i can be directly determined by measuring the phase retardation $\phi_i \sim \mathrm{Im}[t_j/t_k] = (2\pi/\lambda_L)\Delta n_i l_{\mathrm{GaAs}}$ (i,j,k = cyclic permutation of x,y,z) between two beams with polarization along the perpendicular direction j and k. The approximation in the previous expression is valid when $\phi \ll 1$. The depth dependence of the strain field displayed in Fig. 2(a) makes ϕ_i a linear function of z. In the experiments, the diameter of the light beam was chosen so as to illuminate the substrate homogeneously along the z direction. Since the strain-induced changes in the refractive index are very small, their influence on the distribution of the light electric field in the substrate is expected to be negligible. In this case, the phase shift ϕ_i becomes proportional to the average refractive index anisotropy $\Delta\overline{n_i}$ defined in Eq. 3.

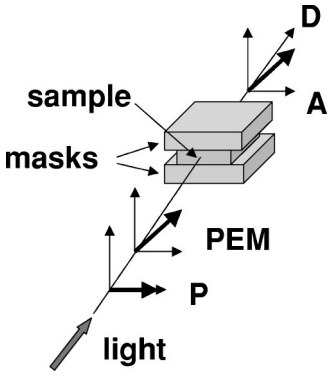

FIG. 3. Experimental setup for TDS measurements in the waveguide geometry: *P*, polarizer; PEM, photoelastic modulator; *A*, analyzer; and *D*, detector. The sample is sandwiched between two masks of opaque material, which prevents stray light from reaching the detector.

The anisotropy $\Delta\overline{n_i}$ was determined by transmission difference spectroscopy (TDS) measurements performed using a photoelastic modulator, in a configuration similar to that reported in Ref. 31 (see Fig. 3). The light source was a monochromatic beam from a Xe lamp filtered by a single monochromator. Unless otherwise specified, the transmission measurements were performed with the monochromator set to the energy of the strong Xe line at $\lambda_L = 990$ nm. A lens with long focal length (18 cm) was employed to focus the light over a wide spot on the cleaved edge of the substrates. In order to block the light propagating around the sample, the latter was sandwiched between masks consisting of polished silicon or germanium blocks. The whole structure was mounted on a temperature-controlled stage (Linkam THMS-600) with temperature stability better than 1 °C. The mounting and the choice of the mask material turned out to be critical for the experiments, as will be described in detail in Sec. IV.

Since the masking blocks may prevent bending of the sample, we used the model of Sec. II to calculate the anisotropy in the refractive index under this particular conditions. For that purpose, we assumed that the masks just counteract the bending force without introducing stress along z (if the masks stress the sample along z, a constant contribution to the anisotropy has to be added to Δn_x and Δn_y). In this case, the strain components ε_{ii} ($i=x,y,z$) do not depend on z. The average strain along z and the integrated anisotropy $\Delta\overline{n_i}$, however, have the same average values as those in Fig. 1(b), thus indicating that the masks do not affect the results presented in the previous section.

Before impinging on the sample, the incident light beam was polarized along the vertical direction by a Glan polarizer *P* and polarization-modulated using a photoelastic modulator (PEM in Fig. 3). The polarization state after transmission was detected using a second Glan polarizer *A* and a silicon photo diode *D*. The angles (θ) relative to the horizontal axis of the polarizer, modulator, and analyzer were set to $\theta_P = 90°$, $\theta_{\mathrm{PEM}} = 45°$, and $\theta_A = 45°$, respectively. If $\delta_M = \delta_0 \cos(\omega_M t)$ denotes the retardation imposed by the PEM, where $\omega_M/(2\pi) = 50$ kHz is the PEM oscillation frequency, the detection intensity for light propagation along the *i* direction becomes

$$I_i=\frac{1}{2}\left[1+\left(\frac{t_{j0}}{t_{k0}}\right)^2+J_0(\delta_0)\right]-\frac{t_{j0}}{t_{k0}}\sin[\phi_i]J_1(\delta_0)\sin(\omega_M t)$$
$$+\frac{1}{2}\left[1-\left(\frac{t_{j0}}{t_{k0}}\right)^2\right]J_2(\delta_0)\cos(2\omega_M t), \quad (5)$$

where $J_l(\delta_0)$ is the lth order Bessel function. The PEM retardation δ_0 was set 2.404 rad to make $J_0(\delta_0)=0$. The signal components with frequencies ω_M and $2\omega_M$, were detected synchronously using a lock-in amplifier. The anisotropy detected in the transmission experiments is very small, so that the transmission ratio $t_{j0}/t_{k0}\sim 1$ and the retardation phase $\phi_i\sim(2\pi\Delta\overline{n_i}l_{\mathrm{GaAs}}/\lambda_L)\ll 1$. In this approximation, ϕ_i becomes proportional to the component of the detected signal at the fundamental PEM frequency ω_M. The great sensitivity of the anisotropic effects arises from the large prefactor $(2\pi l_{\mathrm{GaAs}}/\lambda_L)\sim 10^4$ multiplying $\Delta\overline{n_i}$. The last term of Eq. (5), which is modulated at the second harmonic of the PEM frequency, was found experimentally to be two orders of magnitude smaller than the second term.

C. MOKE measurements

For magneto-optic measurements, the sample was placed in-between a pair of Helmholtz coils used to generate magnetic fields up to ≈ 200 Oe. The magnetization of the MnAs layers was determined through MOKE measurements performed under an incidence angle of 15° in the longitudinal geometry, i.e., with the magnetic field applied along the plane of incidence.[32,33] In order to probe the Kerr effect of the MnAs layers from both the surface and the substrate interface sides, the MOKE experiments were performed using a 940 nm diode laser as the light source. The incident light was polarized along one of the main optical axes along the surface, in order to avoid effects arising from the linear birefringence of the MnAs/GaAs heterostructures. The reflected light passed through a photoelastic modulator (PEM) and through an analyzer prism (A), before being detected by a photodiode. The angles of the optical axes of the PEM and of the analyzer were set to $\theta_{\mathrm{PEM}}=0$ and $\theta_A=45°$, respectively. For this configuration, the intensity of the detected light becomes

$$I=[1+|\Theta_K|^2+2\Theta_K J_0(\delta_0)]+4\,\mathrm{Im}\{\Theta_K\}J_1(\delta_0)\sin(\omega_M t)$$
$$+4\,\mathrm{Re}\{\Theta_K\}J_2(\delta_0)\cos(2\omega_M t), \quad (6)$$

where

$$\Theta_K=r_{sp}/r_{pp}, \quad (7)$$

for the MOKE measurements from the surface and

$$\Theta_K=(t_{ss}/t_{pp})(r_{sp}/r_{pp}) \quad (8)$$

from the substrate. r_{sp} and r_{pp} are the Fresnel reflectivity coefficients. The label s and p indicate the light polarization perpendicular and parallel to the incident plane, respectively. t_{ss} and t_{pp} are coefficients of the transmission through the substrate. Information about the magnetization is included in the coefficient r_{sp}, which is proportional to the off-diagonal component Q of the dielectric tensor induced by the sample magnetization.[32,33]

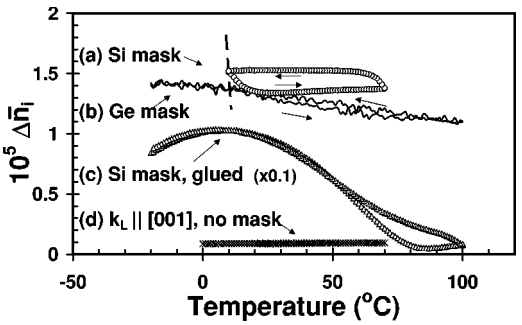

FIG. 4. Refractive index anisotropy $\Delta\overline{n_x}$ as a function of temperature measured on GaAs using masking blocks (cf. Fig. 3) of (a) silicon, (b) germanium, and (c) silicon (glued on the GaAs sample). (d) Δn_z obtained without masking blocks for $k_L||[001]$.

IV. RESULTS

A. Sample mounting considerations

The mounting of the MnAs/GaAs sample within the opaque masks for the transmission experiments (cf. Fig. 3) turned out to be a critical step for the TDS measurements. Figure 4 displays the temperature dependence of the effective anisotropy $\Delta\overline{n_i}$ of pure GaAs measured by TDS under different experimental conditions. Figure 4(d) was recorded for light propagating with wave vector k_L along the $z||[001]$ axis. No masks are required in this case. Since GaAs is optically isotropic for $k_L||[001]$, the small signal ($\Delta\overline{n_z}\sim 2\times 10^{-6}$) detected in Fig. 4(d) is attributed to misalignment and to the strain introduced during sample mounting.

The other curves in Fig. 4 were recorded in the wave guide geometry with $k_L||x||[110]$. In the first experiments, the samples were glued to Si masking blocks using a wax with high softening temperature ($\approx 150\,°\mathrm{C}$). This procedure turned out to be inappropriate because the wax introduces a high strain field in the GaAs, as illustrated in Fig. 4(c) (note the scaling by 0.1). The subsequent experiments were then performed by using a small spring to fix the GaAs in-between the masking blocks. When Si masks were used, we observed that, while the anisotropy reduces significantly, the $\Delta\overline{n_x}$ curves show a strong hysteresis with temperature [cf. Fig. 4(a)]. The hysteresis is attributed to the strain induced in the GaAs by the difference in thermal expansion coefficients of GaAs ($\alpha_{\mathrm{GaAs}}=6.8\times 10^{-6}/\mathrm{K}$) and Si ($\alpha_{\mathrm{Si}}=2.6\times 10^{-6}/\mathrm{K}$).[20] The dashed line displays the expected variation in $\Delta\overline{n_x}$ calculated under the assumption that the strain is completely transferred across the contact surface between Si and GaAs. When the sample is heated, a biaxial strain builds up in the GaAs wafer, until it begins to slide relative to the Si blocks. As the temperature further increases, the two materials slide relative to each other. The friction forces between them lead to a constant strain level in GaAs. Note that the direction of the hysteresis loop is consistent with the temperature dependence indicated by the dashed lines.

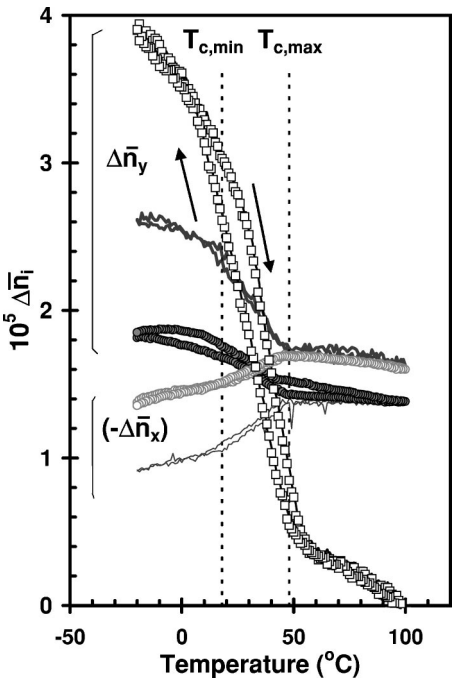

FIG. 5. Temperature dependence of the refractive index anisotropies $-\Delta\overline{n_x}$ and $\Delta\overline{n_y}$ for samples A (lines), B (circles), and C (squares, only $\Delta\overline{n_y}$).

The hysteresis loop can be suppressed by using a mask material with thermal expansion coefficients similar to GaAs. This is demonstrated in Fig. 4(b), which displays results obtained using Ge masking blocks. The thermal expansion coefficient of Ge (6×10^{-6}/K) (Ref. 20) is almost matched to that of GaAs, thus leading to very small hysteresis loops. The subsequent experiments on MnAs/GaAs structures were then performed using Ge masks.

The anisotropy $\Delta\overline{n_x}$ in Fig. 4(b) for $k_L||[110]$ is almost an order of magnitude larger than that measured for $k_L||[001]$ [curve (d)]. GaAs is intrinsically anisotropic for light propagating along $k_L||[110]$ due to spatial dispersion effects.[19] The intrinsic anisotropy ($\Delta n_x = 1.5\times10^{-5}$ at a light wavelength of 990 nm) (Ref. 19) compares well with that measured in Fig. 4(b). This result also indicates that the small spring used to fix the sample induces negligible strain along the *z*-axis.

B. Strain in MnAs/GaAs heterostructures

Figure 5 displays the temperature dependence of $-\Delta\overline{n_x}$ and $\Delta\overline{n_y}$ for the samples A (lines), B (circles), and C (squares, only $\Delta\overline{n_y}$) around the MnAs magnetic phase transition temperature. The temperature dependence of $\Delta\overline{n_x}$ and $\Delta\overline{n_y}$ is attributed to the strain induced in the GaAs substrate by the MnAs film. The difference $\Delta\overline{n_z}=(-\Delta\overline{n_x})-\Delta\overline{n_y}$ directly evidences the anisotropic nature of the strain induced in the substrate as the temperature changes. The elasto-optic origin of the anisotropy is further supported by the spectral dependence of $\Delta\overline{n_i}$ (not shown here). These measurements show that $\Delta\overline{n_i}$ changes sign as the photon energy crosses the isotropic point,[34] which is located just below the GaAs band gap. We also analyzed the stability of the signal during the phase transition with time. The $\Delta\overline{n_i}$ variation measured during 1/2 h at a fixed temperature was $<10\%$, which is of the same order of magnitude as the experimental precision limit.

The temperature profiles in Fig. 5 exhibit three different regions limited by the vertical dashed lines, where the temperatures $T_{c,\min}$ and $T_{c,\max}$ denote the limits of the magnetic phase transition of the MnAs layers in the epitaxial MnAs/GaAs structures.[17] In contrast to the bulk, the phase transition in the heterostructures is not abrupt, but extends over a temperature range $T_{c,\max}-T_{c,\min}\sim30\,^{\circ}$C. $T_{c,\min}$ and $T_{c,\max}$ vary slightly from sample to sample (cf. Table I), the values indicated in Fig. 5 correspond to those measured for sample A. The $\Delta\overline{n_i}$ vs T plots also show a hysteresis loop, whose width also varies from sample to sample. To account for this effect, the $T_{c,\min}$ and $T_{c,\max}$ in Table I were determined for increasing temperatures. Note that the direction of the hysteresis loop is opposite to that observed for the GaAs sample with Si mask shown in Fig. 4(a).

The range $T_{c,\min}-T_{c,\max}\sim30\,^{\circ}$C is close to that reported in Ref. 17. Within this range, $\Delta\overline{n_y}$ ($-\Delta\overline{n_x}$) decreases (increases) linearly with increasing temperature. This behavior is attributed to the increase of the GaAs refractive index n_x relative to n_y when the substrate is compressed along the *x*-direction (see, e.g., Fig. 1). For $T>T_{c,\max}$, $\Delta\overline{n_i}$ varies significantly from sample to sample. Such a variation is expected if the substrates are under different strain levels for temperatures above the phase transition (as a consequence, for instance, of the different layer thickness ratios $d_{\mathrm{MnAs}}/d_{\mathrm{GaAs}}$). This mechanism, however, cannot completely explain the variation, which may also included a contribution from systematic sample misalignment and polarization mixing at imperfections at the cleaved edges of the substrate. Note, however, that the latter do not influence the temperature dependence of $\Delta\overline{n_i}$.

In order to compare the temperature dependence of $\Delta\overline{n_i}$ for different samples, we replot in Fig. 6 the data from Fig. 5 by (i) scaling the curves by the thickness ratio $d_{\mathrm{MnAs}}/d_{\mathrm{GaAs}}$ and (ii) subtracting the corresponding value at $T=100\,^{\circ}$C in order to remove the systematic errors mentioned above. The normalization by the thickness ratio accounts for the fact that the strain levels induced by the MnAs film is expected to be proportional to its thickness and inversely proportional to d_{GaAs}. We observed a very similar behavior for the optical anisotropy as a function of the temperature for all samples. The measured anisotropy is also in good agreement with the theoretical results calculated using the procedure described in Sec. II, which are shown by the diamonds connected by dashed lines. We conclude from these experiments that no appreciable relaxation of the in-plane strain in the MnAs takes place during the phase transition for film thicknesses in the range from 0.10 to 0.25 μm.

C. Magnetic properties of MnAs/GaAs heterostructures

In order to obtain information about the role of the magnetic field on the optical anisotropy, the experiments described in Sec. IV B were also performed under the influence of a magnetic field. No variation in the temperature depen-

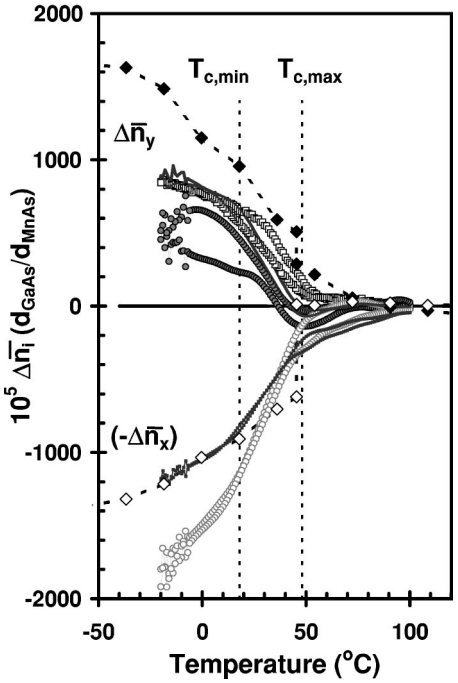

FIG. 6. Temperature dependence of the normalized refractive index $-(d_{\mathrm{GaAs}}/d_{\mathrm{MnAs}})\Delta\overline{n}_x$ and $(d_{\mathrm{GaAs}}/d_{\mathrm{MnAs}})\Delta\overline{n}_y$ for samples A (lines), B (circles), and C (squares). The diamonds connected by dashed lines represent the values calculated using the procedure described in Sec. II.

dence of $\Delta\overline{n}_i$ $(i=x,y)$ profiles was observed for magnetic fields up to 150 Oe applied along directions perpendicular to that of light propagation. This result corroborates the elasto-optic (rather than magneto-optic) nature of the changes in optical anisotropy reported in the previous section.

In the following, we relate the elastic properties of the heterostructures to the magnetic properties of the MnAs films. For that purpose, the magnetization of the MnAs film close to the front surface and close to the interface with the GaAs substrate was probed using the MOKE. The measurements were performed using a laser emitting at the wavelength $\lambda_L=940$ nm, for which the GaAs substrate is transparent. Both the real [proportional to the $2\omega_M$ component of the MOKE intensity cf. Eq. (6)] and the imaginary (proportional to the ω_M component) parts of the Kerr rotation angle Θ_K were measured. Both components show the same functional dependence on temperature and on magnetic field, as expected from the fact that they are proportional to the magneto-optical constant Q. We will concentrate on the real (imaginary) part of MOKE rotation angle, which was found to be the largest component for the front (back) surfaces and will be denoted in the following simply as θ_K (θ_B). Figure 7 displays the Kerr rotation angle for sample A in the ferromagnetic phase ($T=10\,^{\circ}\mathrm{C}$) as a function of the magnetic field. The measurements were performed from the front (closed circles) and from the back surfaces (opened circles) of the MnAs film. The dependence on the magnetic field is similar in the two cases. The abrupt hysteresis loops indicate the good magnetic quality of the two MnAs surfaces. The

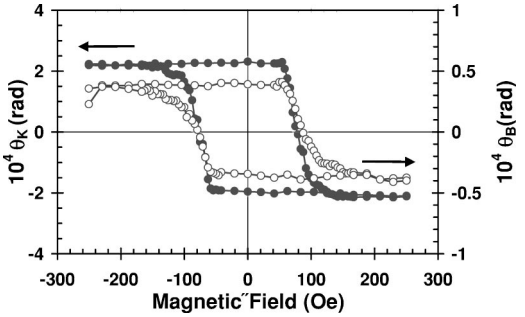

FIG. 7. Real part of the Kerr rotation angle θ_K for sample A measured at 10 °C from the MnAs front surface (front surface, closed circles). The corresponding data for the imaginary part of the Kerr rotation angle measured from the MnAs/GaAs interface (back surface, corresponding to θ_B) is shown by the opened circles.

coercive field for both surfaces is of only 40 Oe, which is one order of magnitude smaller than that for bulk MnAs.[12]

The MOKE rotation angles from the MnAs/GaAs interface are almost 5 times smaller than those measured on the front surface of the MnAs films. The large ratio between the Kerr rotation angles for the front and back surfaces is presently not understood. In fact, if we consider the corrections due to differences in incidence angle at the magnetic film (air and GaAs substrate) for two configurations, we estimate the ratio between the saturation values of the Kerr rotation angles to be

$$\left|\frac{\theta_B}{\theta_K}\right|_{\mathrm{sat}} \sim n_{\mathrm{GaAs}}\left|\frac{n_{\mathrm{MnAs}}^2-1}{n_{\mathrm{MnAs}}^2-n_{\mathrm{GaAs}}^2}t\right|. \tag{9}$$

Assuming that due to its metallic character the imaginary part of refraction index is expected to be larger than the real part, the ratio above becomes of the order of the GaAs refractive index (of approximately 3), where $|t|\sim 1$ is the ratio of the transmission coefficients for the light propagating through the GaAs substrate. Further investigations are required to clarify why the estimated ratio is much larger than the measured one.

The correlation between the elastic and magnetic properties of the MnAs/GaAs structures is summarized in Fig. 8, which compares the temperature dependence of $\Delta\overline{n}_i$ (circles) and of the amplitude $\Delta\theta_K$ (triangles) of the hysteresis loop obtained from MOKE measurements. $\Delta\theta_K$ denotes the difference between the reminiscent Kerr rotation angles θ_K after application of positive and negative magnetic fields oriented along the easy magnetization axis. The MOKE measurements were performed from the front side of the MnAs film using an excitation wavelength of 635 nm. We also included in Fig. 8 the temperature dependence of the average magnetization m, which was obtained using a SQUID magnetometer with the sample subjected to a magnetic field $H=150$ Oe. The temperature range of the hysteresis loop is approximately the same for the SQUID and optical anisotropy data, thus indicating a similar temperature behavior for the magnetic and structural phase transitions. Although the circulation direction of the hysteresis loop is the same for all measurements (see also data for sample C in Fig. 5), the loop

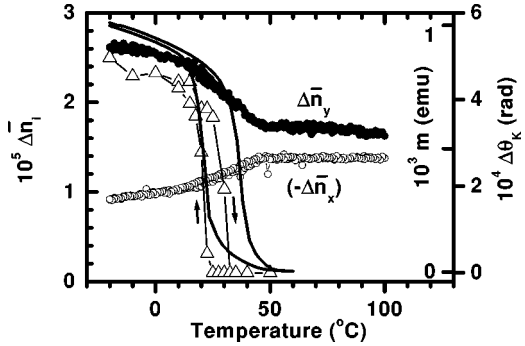

FIG. 8. Temperature dependence of the optical anisotropy ($\Delta\bar{n}_x$ and $\Delta\bar{n}_y$, circles) and of the MOKE (triangles) and SQUID magnetization m (solid line) magnetizations for sample A. The magnetization obtained from the MOKE data is expressed in terms of the difference $\Delta\theta_K$ (triangles) between the reminiscent Kerr rotation angles measured after application of positive and negative magnetic fields. The SQUID magnetization m was measured under a field $H=150$ Oe.

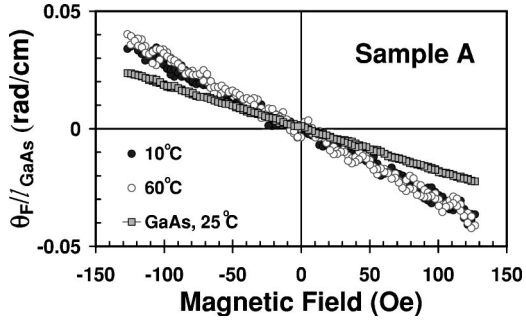

FIG. 9. Faraday rotation angle as a function of the magnetic field in the GaAs reference sample (recorded at $T=25\,^{\circ}$C) and in sample A at $T=10\,^{\circ}$C (ferromagnetic phase of MnAs) and $60\,^{\circ}$C (paramagnetic phase).

is more abrupt and narrow in the MOKE measurements. This difference is attributed to the fact that while the SQUID and optical anisotropy measurements probe average values of the magnetic and structural properties of the MnAs/GaAs heterostructures, respectively, the MOKE experiments detect the magnetization within a thin layer close to the MnAs surface (the skin depth is expected to be of the order of 20 nm). The lower onset temperature of the ferromagnetic/paramagnetic phase transition observed in the MOKE data of Fig. 8 indicates that the nucleation of this phase transition occurs at a lower temperature near the surface than in the bulk of the MnAs films. These results are compatible with a lower stability of the ferromagnetic phase near the surface of the MnAs films.

Finally, we also investigated Faraday rotation in MnAs/GaAs structures by performing polarization-sensitive transmission measurements with the magnetic field and light propagation direction parallel to the easy magnetization axis of the MnAs. The magneto-optical effects are in this case contained in the off-diagonal elements of the transmission coefficient tensor, which leads to a rotation (Faraday rotation) of the light electric field [the expression for the Faraday rotation angle θ_F is similar to Eq. (6) with θ_K replaced by θ_F]. Figure 9 compares the Faraday rotation angle θ_F (normalized to the length l_{GaAs} of the light propagation path) measured for pure GaAs (squares) and for sample A in the ferromagnetic ($T=10\,^{\circ}$C, dots) and in the paramagnetic phase ($T=60\,^{\circ}$C, circles). In all cases, θ_F varies linearly with the magnetic field as expected.[35] Faraday rotation in GaAs is slightly weaker than in MnAs/GaAs structures. However, we did not observe any changes in the Faraday rotation angle of the MnAs/GaAs structures below and above the ferromagnetic phase transition. This result indicates that the contribution from the magnetization of the MnAs film to the Faraday rotation in the substrate is negligible in comparison with that induced by the applied magnetic field.

V. DISCUSSIONS

The TDS experiments described in Sec. IV clearly show that the optical anisotropy induced in the GaAs substrate of MnAs/GaAs structures is of elasto-optic rather than of magneto-optic origin. The MnAs film thus induces significant strain on the GaAs substrate during the phase transition. The strain originates from differences in (i) thermal expansion coefficients between MnAs and the substrate and (ii) in the MnAs lattice parameter below and above the phase transition. The different anisotropies $\Delta\bar{n}_x$ and $\Delta\bar{n}_y$ in Figs. 5 and 6 indicate different strain components ϵ_{xx} and ϵ_{yy} in the plane of the MnAs/GaAs interface. The film/substrate system must thus bend with different radii of curvature along the x and y direction.

The strain levels scale with the thickness of the MnAs film. The magnitude of the strain-induced anisotropy compares well with the theoretical model developed in Sec. II for the whole range of MnAs film thicknesses investigated here (cf. Fig. 6). This result shows that the strain field is transmitted across the interface with the substrate without relief due to the creation of misfit dislocations. We attribute this behavior to the fact that dislocations either cannot nucleate or remain immobile in this low temperature range, as has been suggested from high-resolution transmission electron microscopy and electron diffraction studies of the interface.[13] The experimental data also confirm the nonabrupt nature of the ferromagnetic phase transition in MnAs/GaAs structures,[17] which extends over a range $T_{c,\max}-T_{c,\min}\sim 30\,^{\circ}$C. (Note that the latter is not taken into account by the model of Sec. II.)

A second important aspect investigated here is the relationship between the elastic and magnetic properties of the MnAs/GaAs heterostructures. As mentioned before, the strain field induced in the substrate displays a nonabrupt behavior over the temperature range of the MnAs α-MnAs/β-MnAs phase transition. The magnetization of the film, obtained using a SQUID, shows a similar temperature dependence of the magnetic properties. The phase transition, however, appears to be more abrupt and to take place over a much smaller temperature range when detected by MOKE measurements from the film surface (cf. Fig. 8). These results suggest that the magnetic property phase transition of the MnAs film are inhomogeneous along the growth direction. The inhomogeneity can account for the discrepancy between the SQUID (TDS) and MOKE data, since the former measures the average magnetization (strain induced by the

MnAs film), whereas the latter detects the magnetization locally at the surface.

Finally, the relationship between elastic and magnetic properties of the MnAs layers should allow for the control of the strain field by an external magnetic field. This effect has been previously demonstrated in bulk MnAs films using magnetic fields in the hundreds of Oe range.[12] In the present experiments, we could not detect any dependence of the strain field on an applied magnetic field for field amplitudes up to 200 Oe. This result is attributed to the large magnetic anisotropy of the MnAs layers in MnAs/GaAs structures, which constrains the magnetization along the MnAs *a*-axis for the low fields used in the present experiments. To understand this point, we recall that the size of the magnetic domains in the MnAs/GaAs heterostructures is much larger than the thickness of the MnAs film.[15] Since magnetostriction is a function only of the direction (and not of the sign) of the field,[24] it does not depend on whether the domains are randomly oriented along the *a*-axis or whether they are forced to lie along the $+a$ or $-a$-axis of MnAs by the applied field. Thus, effects of the external field on the elastic properties are only expected for fields sufficiently high to change the magnetization direction or the temperature of the phase transition.

VI. CONCLUSIONS

Optical, magneto-optical, and magnetic properties of epitaxial MnAs/GaAs heterostructures were studied using transmission difference spectroscopy, magneto-optical, and SQUID techniques. The difference between the thermal expansion coefficient of the two materials and the variation of the lattice parameter of MnAs during the ferromagnetic phase transition induces an anisotropic strain field in the GaAs substrate. The latter was detected using polarization-sensitive light transmission measurements through the GaAs substrate. From the comparison between experiments and calculations of the strain distribution using an elastic model for the heterostructures, we conclude that the strain induced during the phase transition is transferred across the film/substrate interface without relaxation through the creation of misfit dislocations. The temperature range of the structural phase transition probed in the optical experiments coincide with that of the magnetic phase transition detected using a SQUID. Magneto-optical Kerr effect measurements give, in contrast, smaller temperature range, which is attributed to a lower stability of the ferromagnetic phase near the surface of the MnAs layers.

ACKNOWLEDGMENTS

We thank V. M. Kaganer and A. Trampert for many helpful discussions, as well as H. v. Kiedrowski, H.-P. Schönherr, and M. Knobel for assistance in the preparation of the samples and in the MOKE and SQUID measurements. We are also indebted to R. Koch and F. Cerdeira for comments and H. T. Grahn for a careful reading of the manuscript. F. I. acknowledges the financial support from the Alexander von Humboldt Foundation and from the Fundação Coordenação de Aperfeiçoamento de Pessoal de Nível Superior (CAPES).

*Electronic address: Iikawa@ifi.unicamp.br

[1] C.J. Palmstrom, Annu. Rev. Mater. Sci. **25**, 389 (1995).
[2] J.W. Orton and C.T. Foxon, Rep. Prog. Phys. **61**, 1 (1998).
[3] M. Tanaka, J.P. Harbison, M.C. Park, Y.S. Park, T. Shin, and G.M. Rothberg, J. Appl. Phys. **76**, 6278 (1994).
[4] M. Tanaka, J.P. Harbison, M.C. Park, Y.S. Park, T. Shin, and G.M. Rothberg, Appl. Phys. Lett. **65**, 1964 (1994).
[5] F. Schippan, A. Trampert, L. Däweritz, and K.H. Ploog, J. Vac. Sci. Technol. B **17**, 1716 (1999).
[6] F. Schippan, A. Trampert, L. Däweritz, K.H. Ploog, B. Dennis, K.U. Neumann, and K.R.A. Ziebeck, J. Cryst. Growth **201/202**, 674 (1999).
[7] B.T.M. Willis and H.P. Rooksby, Proc. Phys. Soc. London, Sect. B **67**, 290 (1954).
[8] N. Menyuk, J.A. Kafalas, K. Dwight, and J.B. Goodenough, Phys. Rev. **177**, 942 (1969).
[9] A. Zieba, Y. Shapira, and S. Fouer, Phys. Lett. **91A**, 243 (1982).
[10] A. Zieba, R. Zach, H. Fjellvag, and A. Kjekshus, J. Phys. Chem. Solids **48**, 79 (1987).
[11] O. Beckmann and L. Lundgren, in *Handbook of Magnetic Materials*, edited by K. H. J. Buschow (North–Holland, Amsterdam, 1991), Vol. 6.
[12] V.A. Chernenko, L. Wee, P.G. McCormick, and R. Street, J. Appl. Phys. **85**, 7833 (1999).
[13] A. Trampert, F. Schippan, L. Däweritz, and K.H. Ploog, Appl. Phys. Lett. **78**, 2461 (2001).
[14] Despite the structural change from hexagonal to orthorhombic at $\approx 125\,^{\circ}$C and from orthorhombic to hexagonal at $\approx 40\,^{\circ}$C, we will use throughout the hexagonal denomination to denote the crystalline axes of the MnAs layers over the whole temperature range.
[15] F. Schippan, G. Behme, L. Däweritz, K.H. Ploog, B. Dennis, K.U. Neumann, and K.R.A. Ziebeck, J. Appl. Phys. **88**, 2766 (2000).
[16] G.A. Govor, Sov. Phys. Solid State **23**, 841 (1981).
[17] V.M. Kaganer, B. Jenichen, F. Schippan, W. Braun, L. Daweritz, and K.H. Ploog, Phys. Rev. Lett. **85**, 341 (2000).
[18] S.H. Chun, S.J. Potashnik, K.C. Ku, J.J. Beny, P. Schiffer, and N. Samarth, Appl. Phys. Lett. **78**, 2530 (2001).
[19] P.Y. Yu and M. Cardona, Solid State Commun. **9**, 1421 (1971).
[20] *Landolt–Börnstein Tables*, edited by O. Madelung (Springer-Verlag, Heidelberg, 1982), Vol. 17a.
[21] *Landolt–Börnstein Tables*, edited by K.H. Hellwege (Springer-Verlag, Heidelberg, 1979), Vol. 11.
[22] T.F. Retajczyk and S.A. Sinha, Appl. Phys. Lett. **36**, 161 (1980).
[23] M.M. de Lima, Jr., R.G. Lacerda, J. Vilcarromero, and F.C. Marques, J. Appl. Phys. **86**, 4936 (1999).
[24] E.T. de Lacheisserie, *Magnetostriction: Theory and Applications of Magnetoelasticity* (CRC, Boca Raton, 1993).
[25] G.A. Govor, K. Bärner, and J.W. Schünemann, Phys. Status Solidi A **113**, 403 (1989).
[26] M. Dörfler and K. Bärner, Phys. Status Solidi A **17**, 141 (1973).
[27] K. Bärner and H. Berg, Phys. Status Solidi A **49**, 545 (1978).
[28] H. Okamoto, in *Binary Allow Phase Diagrams*, edited by T.B. Massalski, H. Okamoto, P.R. Subramanian, and L. Kacprzak

(American Society of Metals, Metals Park, Ohio, 1990), Vol. 1.
[29] L.D. Landau and E.M. Lifschitz, *Lehrbuch der Theoretischen Physik VII - Elastizittstheorie* (Akademia, Berlin, 1965).
[30] J. Sirotin and M.P. Shaskolskaya, *Fundamentals of Crystal Physics* (Mir, Moscow, 1982).
[31] B. Koopmans, P.V. Santos, and M. Cardona, Phys. Status Solidi B **205**, 419 (1998).
[32] R.P. Hunt, J. Appl. Phys. **38**, 1652 (1967).
[33] C.-Y. You and S.-C. Shin, J. Appl. Phys. **84**, 541 (1998).
[34] M. Cardona, in *Atomic Structure and Properties of Solids*, edited by E. Burstein (Academic, New York, 1966), p. 514.
[35] H. Piller, in *Semiconductors and Semimetals*, edited by R.K. Willardson and A.C. Beer (Academic, New York, 1972), Vol. 8.